Proceedings of the ASME 2023 19th International Manufacturing Science and Engineering Conference
MSEC2023
June 12-16, 2023, New Brunswick, New Jersey, USA

MSEC2023-105092

MIXING OF SPHERICAL SOLID AND NANOPOROUS COPPER POWDERS AS LOW-REFLECTANCE FEEDSTOCK FOR LASER POWDER BED FUSION

Natalya Kublik
Arizona State University, AZ

Stanislau Niauzorau
Arizona State University, AZ

Bruno Azeredo
Arizona State University, AZ

ABSTRACT

Micro- and nanoporous materials have gathered attention from the scientific community due to their size dependent properties, including but not limited to high specific surface area, surface diffusivity, bulk diffusivity and permeability, catalytic activity, and distinct optical properties. In this work, spherical nanoporous copper (np-Cu) powders, due to their nanosized porosity and low Cu_2O content, show hemispherical total reflectance of 20% which is significantly lower than its bulk counterpart value for solid or molten copper of approximately 97% at wavelengths of most commercial Laser Powder Bed Fusion (L-PBF) commercial machines. The low-reflectance of np-Cu powders has the potential to be used in L-PBF to improve laser absorption, volumetric energy efficiency, and throughput of this additive manufacturing process. In fact, a prepared mixture of solid Cu powders containing only 5 wt.% of np-Cu powders reflects 34.8 % less than pure copper powders as shown in this paper. Np-Cu powders are fabricated via chemical dealloying of gas atomized CuAl alloy in a robust and scalable approach, and then mixed with pure copper powders to prepare hybrid feedstocks. Under this framework, the crucial role of deglomeration strategies to achieve homogeneity and flowability of np-Cu/Cu hybrid mixtures are evaluated via particle imaging to determine agglomerate size and composition with an eye at obtaining a high-quality print in L-PBF. In np-Cu powders fabrication, washing them in low-surface tension fluids upholds the highest degree of deglomeration in their fabrication process, and for hybrid feedstocks preparation, pre-mixing Cu and CuAl prior to dealloying yields the best homogeneity results with smallest size of agglomerates and good flowability.

Keywords: *Metal additive manufacturing; High absorption LPBF; Feedstock homogeneity, Agglomerates.*

INTRODUCTION

In view of the widely used micro- and nanoporous materials and their size-dependent properties, porous metals have been studied for over 60 years [1] because of their high reactivity and surface area. Nanoporous gold electrodes are used for chemical sensing in the development of immunosensors, biosensors, DNA sensors, and others due to their high surface area, pore size tunability, bi-continuous structure, and preserved electrical conductance [2]. Nanoporous metals have also been applied in semiconducting industry for their electrochemical-mechanical actuation properties with low operating voltages [3], as well as in manufacturing porous light weight batteries with outstanding energy and power density [4]. Lastly, nanostructures also promote higher absorption due to light trapping in nanopores and a graded transition in effective refractive index such as silicon nanowires used in solar cell applications [5]. In additive manufacturing (AM) of metals, low absorption (or high reflectance) remains a challenge for LPBF processes particularly for highly reflective metals such as copper and aluminum considering that most of laser's input (>90%) is reflected by its direct interaction with the melt pool, particularly when the input wavelength is in the near infrared range (e.g., 1070 nm wavelength). Additional energy losses associated with heat conduction across the powder bed and printed layers yield a process with low volumetric energy efficiency [6]. To overcome this issue, studies focused on optimizing laser parameters have incorporated the use of higher power lasers [6], blue and green diode lasers [7], and ultrashort laser pulses [8], and when focused on the feedstock, incorporating alloy impurities [9], nanoparticles [10] and/or surface functionalization to improve the powder's absorption have been common options. It is also worth noting that L-PBF printing at high energy density settings yields melt-pool cavitation and internal reflections of the laser within it leading to improved absorption [11]. In this study, the

objective is to design highly absorbing copper powder feedstocks by preparing homogeneous hybrid mixtures containing nanoengineered porous copper powders that would promote absorption without compromising the feedstock composition in copper prints (Figure 1). As a step towards this objective, this paper explores the preparation means of np-Cu powders and their addition to obtain homogeneous and agglomerate-free hybrid solid Cu and np-Cu (Cu/np-Cu) powder mixtures. In fact, the process of chemical dealloying to synthesize np-Cu powders inherently involves wet etchants that can induce powder agglomerates by surface tension effects during drying steps which can undermine its applicability for L-PBF. Therefore, as a critical step, this paper examines the agglomerate formation process during np-Cu powders synthesis alongside with their homogeneity during mixing processes in order to create a feedstock that ensures good compositional uniformity, dispersion, flowability, low absorption, and spreadability to enable its smooth integration with L-PBF and further studies on its effectiveness in improving laser energy coupling into the powder bed.

Agglomerates affect feedstock flowability for a given average size of particles and particle size distribution [12] as it promotes interlocking effects and can not only be formed in the process flow for manufacturing np-Cu, but also in its mixing step with solid copper powders as later addressed. When in solution, powders agglomerates can form through the mechanisms of adhesion such as electrostatic forces, physical interlocking due to particles morphology and roughness [13], and most importantly due to surface tension and capillarity forces exerted by hydrogen bubbles formed during dealloying that come in contact with the powders in solution exerting capillarity and promoting cluster formation [14], as also shown in Figure 3. Additionally, surface tension becomes a predominant effect during the drying stage by the formation of liquid-vapor-solid interfaces [13]. This study characterizes and compares strategy methods during np-Cu powders preparation and their mixing with pure Cu powders, aiming for the reduction of agglomerates, deglomeration of existing ones, and homogeneity of mixes.

MATERIALS AND METHODS

Nanoporous Copper (np-Cu) Powder Fabrication and Deglomeration Strategies

Spherical Copper-Aluminum ($Cu_{33}Al_{67}$) gas atomized powders were purchased from *Valimet Inc*. as a precursor (Figure 2a), with corresponding particle size distribution provided as follows: D_{10} – 4.36 µm, D_{50} – 11.76 µm, and D_{90} – 28.55 µm. A total of 50 g of the initial alloy (CuAl) was chemically dealloyed in 2500 ml of aqueous Sodium Hydroxide solution ($NaOH_{(aq)}$, 3M) purchased from *Sigma Aldrich*, starting at 50 °C. After 30 minutes of dealloying at a 1g/30s deposition rate, np-Cu powders were washed with 1L of deionized water (DIw) and 200 mL of Anhydrous ethanol (Reagent Grade, *Carolina*) as one of the adopted strategies to disperse agglomerates formed during dealloying process, followed by drying in vacuum oven for 8 h at 90 °C. Figure 2a-d summarizes and illustrates the np-Cu

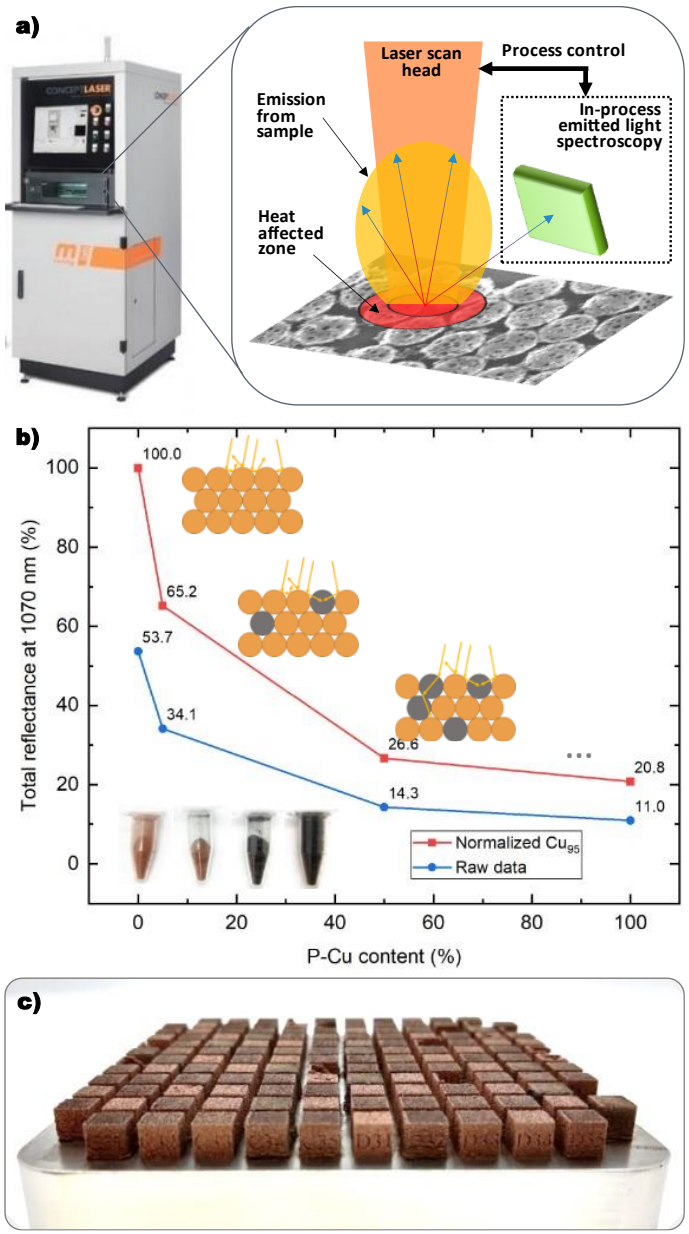

Figure 1. Nanoporous Cu powders low-reflectance property and use in Laser Powder Bed Fusion (LPBF). (a) Graphics of a L-PBF printer and inner laser scan on metal powder bed with high emission from samples. (b) Integrating Sphere total reflectance normalized measurements of pristine and hybrid np-Cu/Cu mixes at laser (1070 nm) wavelength, including insets illustrating decreasing reflectance with increasing np-Cu weight content. (c) Image of a successful L-PBF print of hybrid mix containing 5wt% of np-Cu.

fabrication process via chemical dealloying, from a solid CuAl precursor (Figure 2a) to the hierarchical porous structure of np-Cu (Figure 2b), and to the final dark brown coloration that np-Cu powders present, being associated with their nanoporous morphology and core-shell copper-copper oxide (Cu/Cu_2O)

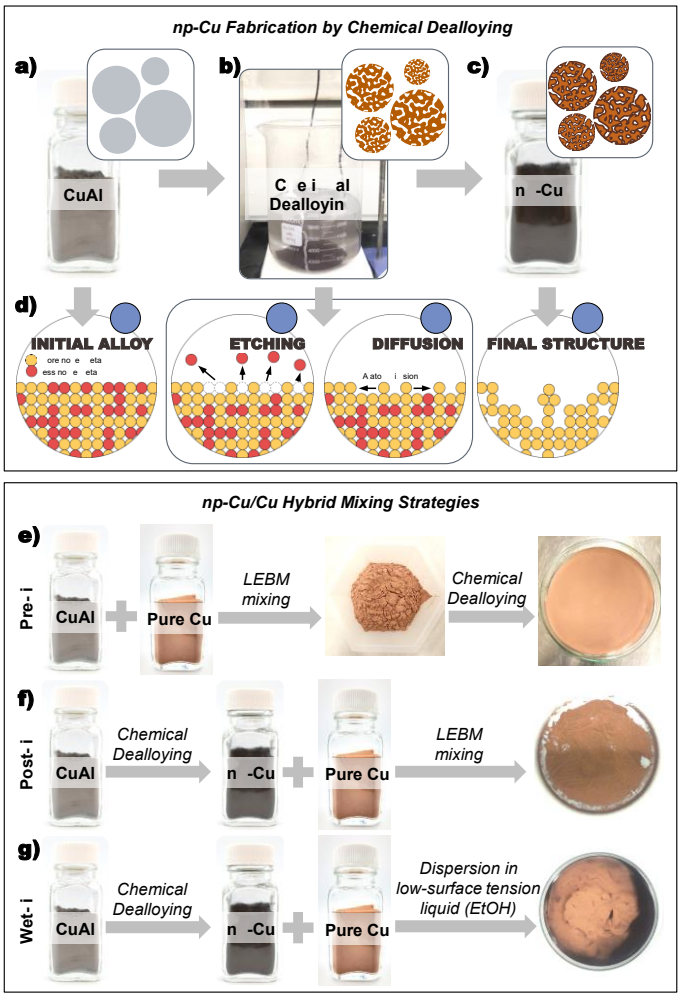

Figure 2. (a-d) Schematics of nanoporous Cu (np-Cu) fabrication: (a) precursor $Cu_{33}Al_{67}$ solid powders, (b) chemical dealloying setup and illustration of np-Cu powders structure during process, (c) np-Cu powder with graphic inset of Cu/Cu_2O core-shell structure of dry powders, and (d) illustration of the kinetics of dealloying process, from solid alloy to porous final structure. (e-g) Flowcharts of mixing strategies to obtain np-Cu/Cu hybrid feedstock, i.e., (e) '*pre-mixing'*, (f) '*post-mixing'*, and (g) '*wet-mixing*' methods.

structure after atmospheric exposure. This figure also illustrates the chemical dealloying process by which Aluminum atoms are etched away and Cu adatoms diffuse along powder's surface to form clusters that eventually form the ligaments of the nanoporous structure (Figure 2d). For the mechanical segregation strategy, sifting with a 60µm sieve step was incorporated at the end of the drying process. In view of promoting the reduction of aggregates formation during the initial stages of chemical dealloying, anionic (SDBS, 0.1387mM) and cationic (CTAB, 0.005mM)) surfactants solutions are individually prepared prior to $NaOH_{(aq)}$ dissolution and CuAl titration.

Hybrid Feedstock Preparation

For np-Cu/Cu hybrid mixtures, gas atomized pure copper powders were purchased from *Praxair Surface Technology* with 99.96% purity and particle size distribution of D_{10} – 22 µm, D_{50} – 34 µm, and D_{90} – 52 µm. In order to obtain homogeneous hybrid feedstocks with minimum agglomerates content, this study explored three preparation means given as: (i) '*pre-mixing'*, (ii) '*post-mixing'* method, and (iii) '*wet-mixing*' methods (See Figure 2e-g).

In the '*pre-mixing'* method shown in Figure 2e, dry pure coper and np-Cu's precursor (CuAl) powders are mechanically mixed with Low Energy Ball-Milling (LEBM, no balls) mixing at 450 rpm for 10 min in forward direction and 10 min in reverse mode. The same LEBM mixing procedure was performed with pure copper and dry np-Cu powders after chemical dealloying, originating the '*post-mixing'* method (see Figure 2f). Lastly, the '*Wet-mixing*' method consists of the mixing of dealloyed np-Cu powders and dry pure copper powders by dispersing both powders in Anhydrous Ethanol at 350 rpm for 5 min and then dried in vacuum oven at 90 °C for 4h (see Figure 2g). Different np-Cu concentrations mixes were prepared for each method, namely: 10wt.%, 15wt.%, 20wt.%, and 40wt.%. In summary, considering the two main sources of agglomeration and inhomogeneity in final hybrid mixes, np-Cu fabrication and mixing for hybrid feedstock preparation, this study analyses optical images to compare the proposed strategies.

Characterization Tools

Optical microscope images for each stage of dealloying and deglomeration strategies during np-Cu fabrication and for each mixing method were obtained with *AmScope* microscope (MU900). Total reflectance (TR) of pure powders and hybrid mix feedstocks were measured with UV/Vis/NIR Spectrometer equipped with integrating sphere (*Perkin Lambda 950*). Flowability was evaluated with Hall and Carney flowmeters indicated by ASTM B213-20 and ASTM B964-16 standard tests, respectively, with 50g used in both tests. The process was

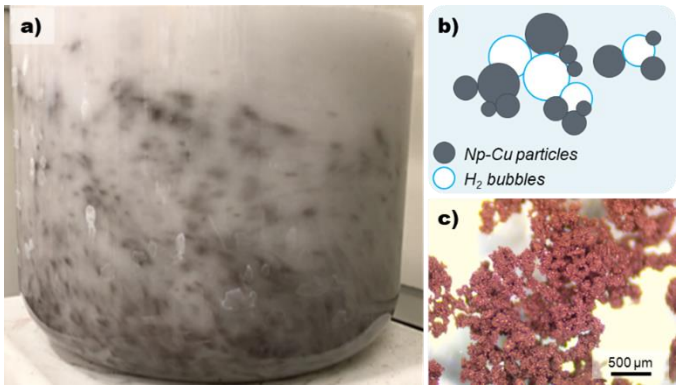

Figure 3. (a) Image of np-Cu powders in $NaOH_{(aq)}$ solution during chemical dealloying process. (b) Illustrated mechanism of np-Cu clusters formation due to capillarity effect with H_2 bubbles generated as a by-product of the dealloying reaction. (c) Optical microscope image of agglomerates formed in $NaOH_{(aq)}$ solution.

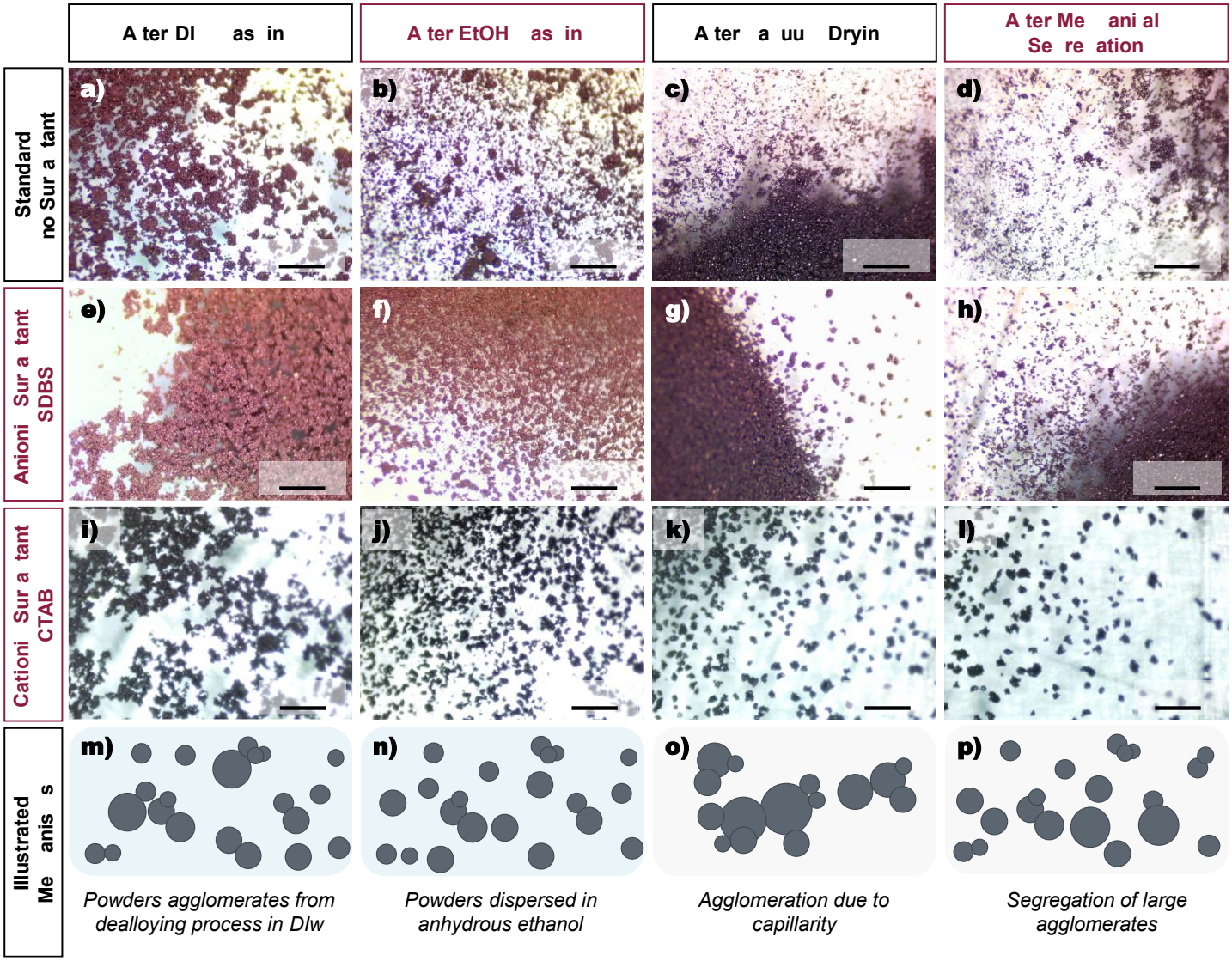

Figure 4. Optical microscope images and illustrated mechanisms of np-Cu powders dispersion for each step of their fabrication using proposed deglomeration methods, as highlighted with red titles. (a-d) Standard fabrication images are shown for comparison to the methods with (e-h) anionic and (i-l) cationic surfactants. Images for in-process strategies such as (b, f, j) anhydrous ethanol (EtOH) wash and (d, h, l) mechanical segregation are also shown in second and fourth columns, respectively. Images in the two first columns were taken powders in DI water and Anhydrous EtOH solutions whereas powders were dry in the last two. Lastly, (m-p) agglomerates formation and segregation mechanisms at each stage of np-Cu fabrication are illustrated in the last row.

repeated 3 times for each sample and both Hall and Carney flowmeter funnels were obtained from *Qualtech* Products Ltd.

RESULTS AND DISCUSSION

The anti-reflective size-dependent property of np-Cu powders and its mixtures with solid copper powders is measured at room temperature by total reflectance measurements as a function of its mixing ratio by '*post-mixing*' method (see Figure 2g). The measurements shown on Figure 1b reveal np-Cu powders' superior anti-reflection compared to pure copper powders as well as a non-linear reduction of reflectance in the mixes with increasing np-Cu powders content. These results are attributed to the light entrapment effects associated with internal reflections and a reduced contrast in effective refractive index between np-Cu and air, and a low content of Cu_2O oxides (<12 at.%) which is highly absorbing in a broad-spectrum. Note that the blue curve in Figure 1b represents raw reflectance data whereas red curve is normalized against the reflectance of pure solid Cu powders at 1070 nm. It is shown that the introduction of 5 wt.% of np-Cu alone can promote a drop from 100% to 65.2% in its normalized reflectance, and to 26.6% when the np-Cu content reaches 50 wt.%. Insets in Figure 1b illustrate the increase in absorption promoted by the addition of np-Cu powders in the feedstock;

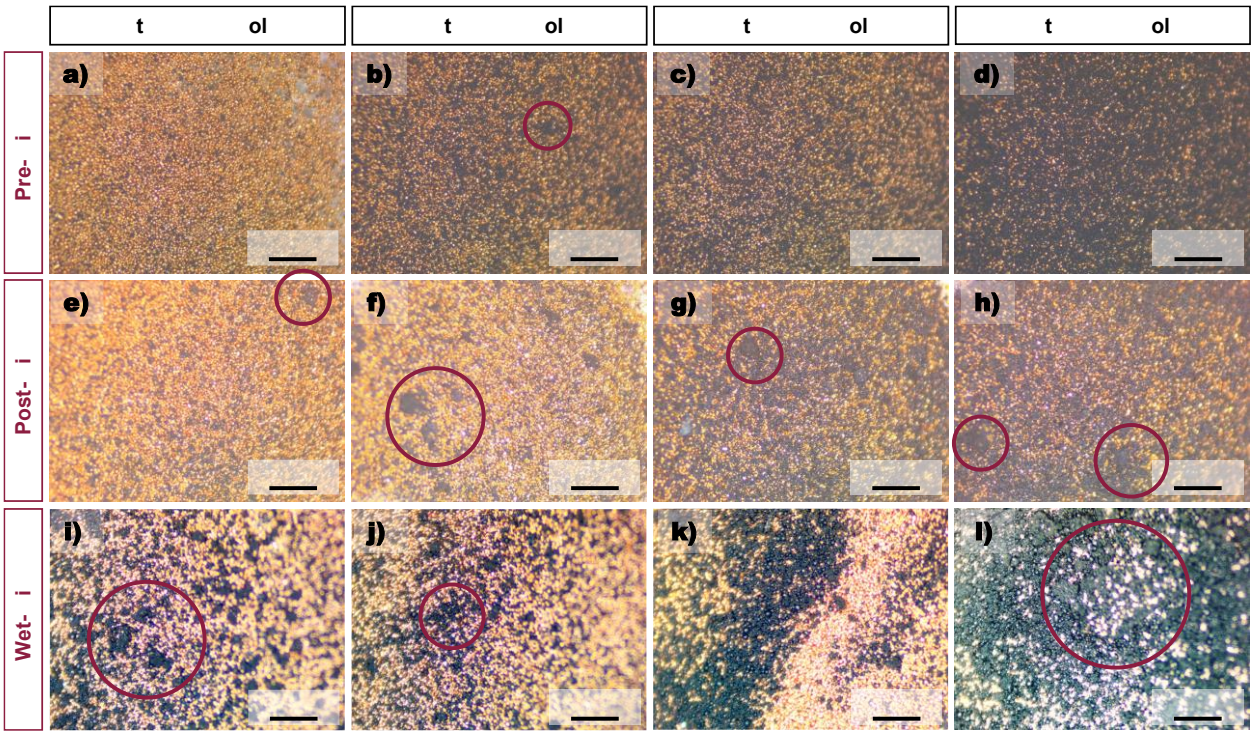

Figure 5. Optical microscope images of hybrid pure Cu/np-Cu prepared feedstocks dispersion by proposed means: (a-d) '*Pre-mix*', (e-h) '*post-mix*', and (i-l) '*wet-mix*', for np-Cu concentrations of 10wt.%, 15 wt.%, 20 wt.%, and 40 wt.%. Red circumferences highlight agglomerates formed.

images of the pure copper, pure np-Cu and hybrid feedstocks with 5 wt.% and 50 wt.% of np-Cu show the darkening of the mixture visible also to the naked eye. Figure 1c shows an image of a successful print performed utilizing a hybrid feedstock print containing only 5 wt.% np-Cu.

In regards to the initial np-Cu fabrication, dispersion imaging results with optical microscope images are shown in Figure 4 for each of the stages of the post-dealloying processes, including deglomeration strategies of immersion in anhydrous ethanol (Figure 4b, f, j, n) and sifting (Ø = 60µm mesh) for mechanical segregation of large clusters (Figure 4d, h, i, p). To remove $NaOH_{(aq)}$ remnant and interrupt the chemical dealloying reaction, powders are first washed with DI water. At this stage, the powders are imaged in liquid (Figure 4a, e, i) and large clusters can be observed. These clusters are expected to have been formed by capillarity effects during the dealloying process by the interaction with hydrogen bubbles (a by-product of the dealloying reaction) with metal powders (Figure 3). Owning to $NaOH_{(aq)}$'s and DI water's high surface tension, powder agglomeration is inevitable. Next, the agglomerate sizes are qualitatively tracked after the subsequent step of 'ethanol (EtOH) washing'. It is possible to see that agglomerate sizes were reduced by EtOH rinsing (see Figure 4b, f, j, n). After the 'vacuum drying' step, capillarity forces bring particles together and can once more promote agglomerate formation, especially of smaller particles as can be seen in Figure 4c, g, k and as illustrated in Figure 4o. 'Mechanical segregation' is introduced by sifting the powders with a 60µm mesh size and is intended to remove or deagglomerate clusters larger than its mesh size. However, on a qualitative level, this approach has had a minor impact on the agglomerate sizes for both the process routes without surfactants and with anionic and cationic surfactants (Figure 4). Lastly, surfactants were added to alter the interparticle adhesion forces in an effort to promote deglomeration during any of the processing steps. However, among these routes, larger agglomerates are found after drying and mechanical segregation steps in surfactant-added samples (Figure 4g-h, k-l), compared to the route without surfactants (Figure 4c-d). Higher concentrations of both surfactants were tested but found to be an impractical procedure as the amount of foam produced associated with the H_2 gas production from the dealloying reaction, inhibits the dispersion of CuAl precursor alloy and thus compromises np-Cu powder fabrication. Moreover, their limited scalability hinders their feasibility, as the surfactant methods required downscaling to 20% of standard np-Cu fabrication yield. Therefore, the standard fabrication approach without mechanical segregation was selected as the method resulting in the least amount and size of agglomerates for np-Cu production. Further quantitative studies through SEM images paired with image analysis, flowability measurements and their origins are necessary to accurately compare methods.

With an eye at reducing reflections in L-PBF, powders made via the 'standard' route are mixed with solid copper powders into hybrid feedstock by three different methods previously described (Figure 2e-g). To harvest its anti-reflective properties, it is important that its mixtures are homogenized after being spread

by a blade. Again, top-down optical microscopy images were collected of dry spread mixtures containing np-Cu and solid copper at weight ratios of 10 wt.%, 15 wt.%, 20 wt.%, and 40 wt.% of np-Cu (Figure 5). Images reveal the presence of clusters sized over 100 µm composed of both np-Cu and pure Cu/np-Cu mixes (see highlighted red circles in Figure 5). In the '*post-mixing*' approach, multiple np-Cu clusters were observed in this method (see Figure 5e-h), which are predominantly originated from np-Cu fabrication prior to their mechanical mixing with pure Cu (see Figure 2f and Figure 4d). The '*wet-mixing*' method presented large clusters of both np-Cu alone and of mixed pure Cu and np-Cu. The latter type of cluster is presumed to have been formed due to capillarity forces during the drying stage of the mixed feedstock and lead to high levels of inhomogeneity (see Figure 5i-l). This inhomogeneity is attributed to hydrodynamic effects that play a role after vigorously mixing them in solution. As dispersed particles begin to decant to the bottom, larger particles decant faster due to reduced drag effects leading to a prominent segregation of both powders (see Figure 2g). By optical microscope analysis alone, '*pre-mixing*' method has demonstrated the smaller amount of agglomerates and superior homogeneity of dispersion among all methods. Furthermore, np-Cu powders addition through this method was also shown to essentialy preserve pure Cu powders flowability. Hall flowability for a 'pre-mix' feedstock containing 5 wt.% of np-Cu was measured as 24.9 s/50g, whereas pure Cu and np-Cu powders flowability were determined as 22.1 s/50g and 32.9 s/50g (Carney flowmeter), respectively.

CONCLUSION

In summary, this study assessed the crucial analysis of agglomerate formation in spherical nanoporous copper (np-Cu) powders fabrication and homogeneity in mixing of pure copper and np-Cu hybrid feedstock for use in Laser Powder Bed Fusion 3D printing. Methods and results included process-structure-property relationship analysis of np-Cu powders in their fabrication by employing the use of anhydrous ethanol to wash powders, surfactants, and mechanical segregation by sifting. Concerning the preparation of np-Cu/Cu hybrid feedstocks, their homogeneity, and agglomerate size and composition were analyzed as a function of three mixing strategies at different stages of the entire process flow. Findings indicate that low-surface tension washing overperform in segregating np-Cu powders agglomerates, whereas in hybrid feedstocks, pre-mixing of pure Cu and CuAl prior to chemical dealloying demonstrated to produce more homogeneous hybrid feedstocks with the least number of agglomerates and preserved flowability. Further qualitative studies are aimed to reinforce observed results. Due to nanosized-dependent properties, np-Cu and mixes exhibit outstanding potential in L-PBF copper prints as np-Cu present reflectance of 20.8% when compared to solid pure Cu feedstock.

ACKNOWLEDGEMENTS

We acknowledge the use of facilities with the LeRoy Eyring Center for Solid State Science at Arizona State University and John M. Cowley High Resolution Electron Microscopy at Arizona State University. We acknowledge the National Science Foundation under Grant No. CMMI-1932899.

REFERENCES

[1] P. B. Weisz and J. S. Hicks Socony, "THE BEHAVIOUR OF POROUS CATALYST PARTICLES IN VIEW OF INTERNAL MASS AND HEAT DIFFUSION EFFECTS."

[2] M. M. Collinson, "Nanoporous Gold Electrodes and Their Applications in Analytical Chemistry," *ISRN Analytical Chemistry*, vol. 2013, pp. 1–21, Feb. 2013, doi: 10.1155/2013/692484.

[3] M. Brinker and P. Huber, "Wafer-Scale Electroactive Nanoporous Silicon: Large and Fully Reversible Electrochemo-Mechanical Actuation in Aqueous Electrolytes," *Advanced Materials*, vol. 34, no. 1, Jan. 2022, doi: 10.1002/adma.202105923.

[4] J. H. Pikul, H. Gang Zhang, J. Cho, P. v. Braun, and W. P. King, "High-power lithium ion microbatteries from interdigitated three-dimensional bicontinuous nanoporous electrodes," *Nat Commun*, vol. 4, 2013, doi: 10.1038/ncomms2747.

[5] E. Garnett and P. Yang, "Light trapping in silicon nanowire solar cells," *Nano Lett*, vol. 10, no. 3, pp. 1082–1087, Mar. 2010, doi: 10.1021/nl100161z.

[6] S. D. Jadhav, L. R. Goossens, Y. Kinds, B. van Hooreweder, and K. Vanmeensel, "Laser-based powder bed fusion additive manufacturing of pure copper," *Addit Manuf*, vol. 42, no. February, 2021, doi: 10.1016/j.addma.2021.101990.

[7] E. Hori, Y. Sato, T. Shibata, K. Tojo, and M. Tsukamoto, "Development of SLM process using 200 W blue diode laser for pure copper additive manufacturing of high density structure," *J Laser Appl*, vol. 33, no. 1, p. 012008, Feb. 2021, doi: 10.2351/7.0000311.

[8] L. Kaden *et al.*, "Selective laser melting of copper using ultrashort laser pulses," *Appl Phys A Mater Sci Process*, vol. 123, no. 9, Sep. 2017, doi: 10.1007/s00339-017-1189-6.

[9] N. Kraiem *et al.*, "Influence of aluminum addition on the laser powder bed fusion of copper-aluminum mixtures," *Additive Manufacturing Letters*, vol. 3, p. 100080, Dec. 2022, doi: 10.1016/j.addlet.2022.100080.

[10] S. D. Jadhav *et al.*, "Influence of carbon nanoparticle addition (and impurities) on selective laser melting of pure copper," *Materials*, vol. 12, no. 15, 2019, doi: 10.3390/ma12152469.

[11] J. v. Gordon *et al.*, "Defect structure process maps for laser powder bed fusion additive manufacturing," *Addit*

Manuf, vol. 36, Dec. 2020, doi: 10.1016/j.addma.2020.101552.

[12] P. Kiani, U. Scipioni Bertoli, A. D. Dupuy, K. Ma, and J. M. Schoenung, "A Statistical Analysis of Powder Flowability in Metal Additive Manufacturing," *Adv Eng Mater*, vol. 22, no. 10, Oct. 2020, doi: 10.1002/adem.202000022.

[13] P. S. Raux and A. L. Biance, "Cohesion and agglomeration of wet powders," *Phys Rev Fluids*, vol. 3, no. 1, Jan. 2018, doi: 10.1103/PhysRevFluids.3.014301.

[14] A. Goldszal and J. Bousquet, "Wet agglomeration of powders: from physics toward process optimization," 2001. [Online]. Available: www.elsevier.comrlocaterpowtec

[15] A. de Vries, Y. Lopez Gomez, B. Jansen, E. van der Linden, and E. Scholten, "Controlling Agglomeration of Protein Aggregates for Structure Formation in Liquid Oil: A Sticky Business," *ACS Appl Mater Interfaces*, vol. 9, no. 11, pp. 10136–10147, Mar. 2017, doi: 10.1021/acsami.7b00443.